Chemisorption theory

253. P. W. Tasker, *J. Phys. C* **1978**, *12*, 4977; *Phil. Mag. A* **1979**, *39*, 119.
254. F. Rohr, K. Wirth, J. Libuda, D. Cappus, M. Bäumer, H.-J. Freund, *Surf. Sci.* **1994**, *315*, L299.
255. D. Cappus. M. Haßel, E. Neuhaus, M. Heber, F. Rohr, H.-J. Freund, *Surf. Sci.*, **1995**, *337*, 268.
256. G. Illing, Thesis, Ruhr-Universität Bochum, **1990**.
257. R. Lacman, *Colloq. Int. CNRS* **1965**, *152*, 195.
258. D. Wolf, *Phys. Rev. Lett.* **1992**, *68*, 3315.
259. C. A. Ventrice Jr., H. Hannemann, Th. Bertrams, H. Neddermeyer, *Phys. Rev. B* **1994**, *49*, 5773.
260. M. P. Kiskinova, *Poisoning and Promotion in Catalysis Based on Surface Science Concepts and Experiments*, Studies in Surface Science and Catalysis Vol. 70, Elsevier, Amsterdam, **1992**.
261. H. P. Bonzel, *Surf. Sci. Rep.* **1987**, *8*, 43.
262. H. P. Bonzel, A. M. Bradshaw, G. Ertl (Eds), *Physics and Chemistry of Alkali Metal Adsorption*, Material Science Monographs Vol. 57, Elsevier, Amsterdam, **1989**.
263. M. P. Kiskinova, G. Pirug, H. P. Bonzel, *Surf. Sci.* **1983**, *133*, 321.
264. M. Scheffler, Ch. Droste, A. Fleszar, F. Máca, G. Wachutka, G. Barzel, *Physica* **1991**, *172B*, 143.
265. L. J. Whitman, W. Ho, *J. Chem. Phys.* **1989**, *90*, 6018.
266. H. Pfnür, P. Feulner, D. Menzel, *J. Chem. Phys.* **1983**, *79*, 4613.
267. J. E. Crowell, E. L. Garfunkel, G. A. Somorjai, *Surf. Sci.* **1982**, *121*, 303.
268. T. E. Madey, C. Benndorf, *Surf. Sci.* **1985**, *164*, 602.
269. F. Sette, J. Stöhr, E. B. Kollin, D. J. Dwyer, J. L. Gland, J. L. Robbins, A. L. Johnson, *Phys. Rev. Lett.* **1985**, *54*, 935.
270. J. L. Gland, R. J. Madix, R. W. McCabe, C. DiMaggio, *Surf. Sci.* **1984**, *143*, 46.
271. W. M. Daniel, J. M. White, *Surf. Sci.* **1986**, *171*, 289.
272. J. C. Bertolini, B. Tardi, *Surf. Sci.* **1981**, *102*, 131.
273. M. Trenary, K. J. Uram, J. T. Yates, Jr., *Surf. Sci.* **1985**, *157*, 512.
274. Xu Zi, L. Surnev, J. T. Yates, Jr., unpublished results.
275. T. Yamada, Z. Runsheng, Ya. Iwisawa, K. Tamaku, *Surf. Sci.* **1988**, *205*, 82.
276. M. Kiskinova, A. Szabo, J. T. Yates, Jr., *J. Chem. Phys.* **1988**, *89*, 7599.
277. M. Kiskinova, A. Szabo, J. T. Yates, Jr., *Surf. Sci.* **1990**, *226*, 237.
278. J. L. Brand, M. V. Arena, A. A. Deckart, S. M. George, *J. Chem. Phys.* **1990**, *92*, 4483.
279. S. Johnson, R. D. Madix, *Surf. Sci.* **1981**, *108*, 77.
280. J. Benziger, R. J. Madix, *Surf. Sci.* **1980**, *94*, 119.
281. M. L. Burke, R. J. Madix, *Surf. Sci.* **1990**, *237*, 1.
282. J. G. Chen, W. Erley, H. Ibach, *Surf. Sci.* **1989**, *224*, 215.

5.1.2 Chemisorption Theory

R. A. VAN SANTEN AND M. NEUROCK

5.1.2.1 Introduction

Computational quantum chemistry and solid state physics have reached the stage where quantitatively reliable predictions on the interaction of small and moderate sized molecules with transition metal clusters or surfaces are now possible. Computation therefore begins to enrich experimental information by providing results of model systems that are not easily accessible to experiment. In addition they allow us to probe the nature of transient surface species such as short-lived intermediates and activated complexes. Nonetheless, the qualitative theoretical framework that has been established over the past 50 years remains highly relevant. It provides a sound framework for conceptual analysis and interpretation. Computation and experiment then can be used to test ideas on the electronic and structural parameters which control the geometry, energetics, and dynamics of the chemisorbed molecule.

Two different schools of thought in chemisorption theory can be distinguished. The first is born out of the solid-state physics community, while the second originates from the theoretical chemistry community. Formal chemisorption theory dates back to the 1950s and 1960s where the relevant electronic factor for chemisorption was considered to be the local electron density of states at the Fermi level. This is especially true in catalysis. Magnetic and conductivity measurements were usually interpreted in these terms. With progress in solid state physics, theory became more refined and surface physicists developed a more physically realistic view of the surface chemical bond. Koutecky [1], Newns [2], Grimley [3], and Schieffer [4] are considered to be the founders of formal chemisorption theory. Many of their concepts remain today and are the basis of our current views on chemisorption. Formal chemisorption theory is therefore the subject of the first section. One of the most important results derived from formal chemisorption theory was the rationalization of strength of adsorbate–surface interaction in terms of the ratio of adsorbate–surface-atom strength versus the interaction energy between the surface atoms. It raised the issue of the existence of the concept of a surface adsorption complex, hence identifying chemisorption physics with surface complex chemistry.

The theoretical chemical application of surface chemical bonding theory, highlighted next, is related to formal chemisorption theory as developed in surface physics, but concentrates on quantum chemical concepts as the electron distribution over bonding and antibonding orbital fragments [5, 6]. It will be seen that both approaches complement each other. The notion of a surface molecule relates to the surface physicists' concept of surface state.

The final section provides an overview of the current understanding of the factors that govern the physical chemistry of chemisorption. Our understanding of the factors that determine the site preference of surface dependence of chemisorption is summarized. We demonstrate many of those concepts through a series of first-principle quantum chemical results on different example systems. The results allow us to specifically quantify different aspects of the interaction, such as

lateral interactions and adsorbate and surface structure relaxation. The first-principle nature of the calculations leads to very good overall comparisons with available experimental data. This chapter focuses specifically on chemisorption to transition metal surfaces.

5.1.2.2 Formal Chemisorption Theory

A Introduction

Quantum theoretical models of chemisorption were initially developed within the framework of two idealized theories of the electronic structure of the solid state:

(i) the tight-binding approximation;
(ii) the jellium model.

In the tight-binding approximation discussed first, the one-electron wave function Ψ_k are considered to be a linear combination of atomic orbitals φ_i:

$$\Psi_k = \sum_i c_i^k \varphi_i \tag{1}$$

This approximation applies best to the d electrons of the transition metals and has been used effectively by the theoretical chemistry community, to study chemisorption. In the free electron or jellium model, discussed in the second section, the one-electron wave functions are, instead, considered as linear combinations of plane waves:

$$\Psi_k(\vec{r}) = \sum_G c(\vec{k} + \vec{G}) e^{i(\vec{k}+\vec{G})r} \tag{2}$$

The jellium model best applies to the s and p valence electrons as in the alkali metals. The consequences of electron–electron interactions are explored effectively. The two approaches can be coupled to form a hybrid model as in effective medium theory [7], where the tight-binding description is used for the d electrons and the jellium approach is used to describe the s and p valence electrons. We will limit the discussion in this chapter to a review of the main results and concepts. A more extensive treatment of the theoretical basis of these methods and derivations is available [6].

B The Tight-Binding Quantum Theoretical Model of Chemisorption

Within the tight-binding approximation (Fig. 1), the general form of the one-electron wave function that describes the electronic structure of the chemisorption system is

$$\Psi_l = \sum_i a_i^l \varphi_i^{ads} + \sum_j a_j^l \psi_j \tag{3}$$

The wave functions ψ_j correspond to the undisturbed substrate, and φ_i^{ads} are the one electron wave functions of the adsorbing molecule.

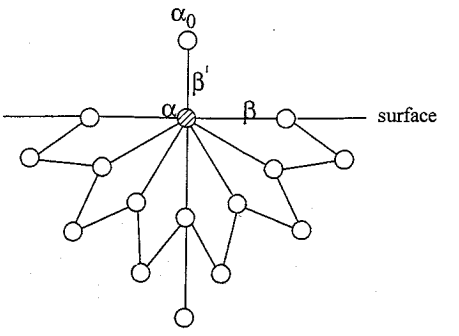

Figure 1. Parameters in the tight-binding model of chemisorption.

In general φ_i^{ads} and ψ_j are nonorthogonal:

$$\int d\tau \varphi_i^{ads} \psi_j = S_{ij}^{ads,met} \neq 0 \tag{4}$$

This nonorthogonality has to be explicitly included into chemisorption theory to account for the Pauli repulsive part of the interaction energy. The quantum-mechanical solution of the chemisorption problem has been found, when the coefficients a_i^l and eigenvalue energies E_l are known. A very useful expression is the local density of states $\rho_i(E)$, that gives the probability of finding an electron with energy E in adsorbate orbital i. In the case where the adsorbate is described by a single atomic orbital φ_0 with energy α_0, the corresponding expression is

$$\rho_0(E) = \frac{1}{\pi} \frac{\Gamma(E)}{(\alpha_0 + \Lambda(E) - E) + \Gamma^2(E)} \tag{5}$$

$\Gamma(E)$ and $\Delta(E)$ are the line width and energy shift functions and are given by

$$\Gamma(E) = \pi \sum_i |\langle \varphi_0 | H | \psi_i \rangle|^2 \delta(E - E_i) \tag{6}$$

$$\Lambda(E) = \sum_i \frac{|\langle \varphi_0 | H | \psi_i \rangle|^2}{E - E_i} \tag{7}$$

Figure 2 depicts the energy dependence of $\rho_0(E)$ sketched as a function of the interaction energy between adsorbate and surface. In the weak adsorption limit, $\Gamma(E)$ and $\Delta(E)$ can be considered energy independent. The maximum electron density of states on the adsorbate appears to be shifted by Λ and is broadened by a Lorentzian distribution over width 2Γ.

The dependence on the interaction energy can be deduced by substituting the expression for tight binding wave function in the bulk

$$\psi_j = \sum_k b_k^j \varphi_k^m \tag{8}$$

References see page 957

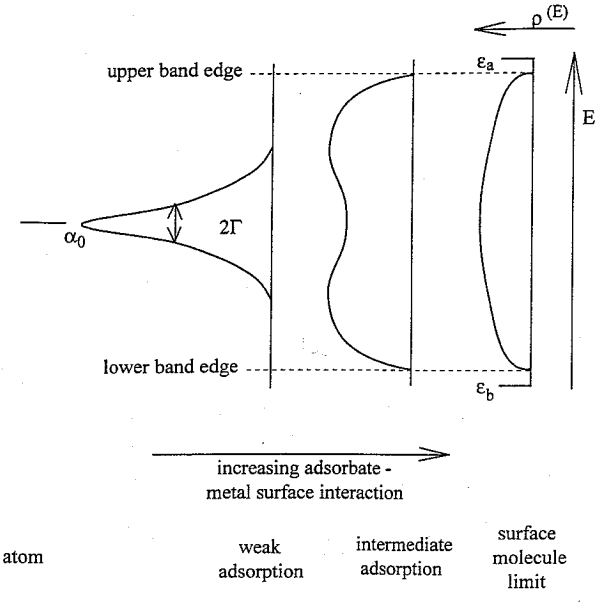

Figure 2. Adsorbate local density of states as a function of adsorbate–metal surface interaction (schematic).

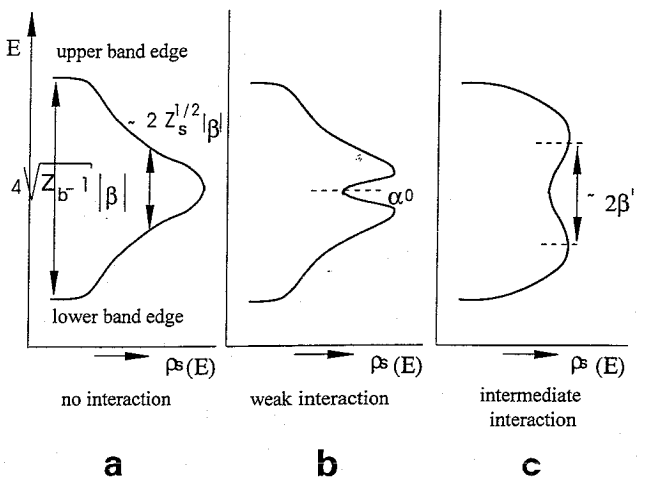

Figure 3. Adsorption-induced changes in the surface local densities of states (schematic).

into eq 5–7 for $\Gamma(E)$ and $\Lambda(E)$. In the situation where the adsorbate orbital φ_0 interacts only with one surface atomic orbital eqs 6 and 7 reduce to

$$\Gamma(E) = \pi\beta'^2\rho_s(E') \tag{9}$$

$$\Lambda(E) = \oint dE' \frac{\Gamma(E')}{E - E'} \tag{10}$$

$$= \sum_i \frac{\beta'^2|b_s^i|^2}{E - E_i} \tag{11}$$

The symbol $\oint$ in eq 10 means that only the principal part of the integration has to be computed. β' is given by

$$\beta' = \langle\varphi_0^{ads}|H|\varphi_{surf}^m\rangle \tag{12}$$

This is the overlap energy integral between the adsorbate orbital and surface atomic orbital $\varphi_s\rho_s(E)$ is the surface local density of states. Its general form, shown here, is similar to eq 5:

$$\rho_s(E) = \frac{1}{\pi}\frac{\Gamma_s(E)}{(\alpha_s + \Lambda_s(E) - E)^2 + \Gamma_s^2(E)} \tag{13}$$

$\Gamma_s(E)$ and $\Lambda_s(E)$ contain the information on the electronic structure of the solid itself, and α_s is the energy of the surface atomic orbital. Expression 13 can only be evaluated analytically by making further simplifying assumptions about the bulk electronic structure. Useful analytical approximate expressions for $\Gamma_s(E)$ and $\Lambda_s(E)$, correct up to the second moment of the electron energy distribution (eqs 6 and 7) are:

$$\Gamma_s(E) = \frac{z_s}{z_b - 1}\sqrt{4(z_b - 1)\beta^2 - (\alpha_s - E)^2};$$

$$(\alpha_s - E)^2 < 4(z_b - 1)\beta^2 \tag{14}$$

$$\Lambda_s(E) = \frac{z_s}{z_b - 1}(E - E_\alpha) \tag{15}$$

where z_s is the number of nearest atom neighbors of the surface atom, z_b is the number of nearest atom neighbors in the bulk, and β the overlap energy integral between metal atomic orbitals (see Fig. 1). The resulting energy dependence of $\rho_s(E)$ is sketched in Fig. 3.

The bulk electrons are contained in an electron band of width

$$4\sqrt{z_b - 1}|\beta|$$

This width describes the degree of delocalization of the bulk electrons. It is proportional to the overlap energy integral of the metal atomic orbitals and increases with the number of metal atom neighbours.

The delocalization of the electrons in the surface is less and, hence, the surface bandwidth is smaller. Substituting expression (13) into (9) leads to the following line width function:

$$\Gamma(E) \approx \pi\frac{\beta'^2}{z_s^{1/2}|\beta|}f(E) \tag{16}$$

In the weak interaction limit,

$$\frac{\beta'^2}{z_s\beta^2} \ll f(E) \approx 1$$

provided that $\alpha_s \approx \alpha_0$. The more general case is discussed in subsection D. It is useful to study the interaction system in this limit.

The local electron density of states on the adsorbate in the weak adsorption limit is sketched in Fig. 2. The

adsorbate orbital electron density is broadened into a Lorentzian distribution around a slightly displaced adsorbate orbital energy α_0. Electrons on the adatom with energy less than α_0 gain in energy compared to the nonchemisorbed situation. Electrons with energy higher than α_0 are destabilized with respect to α_0. The chemisorption energy will therefore depend on the electron distribution of the electrons on the substrate, which effectively determines their distribution over bonding and antibonding fragment orbitals.

In the situation where the single electron of the adatom and the Fermi level (the highest occupied surface orbital) of the metal have the same energy α_0 (prior to chemisorption), the interaction energy equals

$$E_{\text{int}}^{\text{w}}(E_{\text{F}} = \alpha_0) = 2\Gamma \tag{17}$$

$$\approx 2\frac{\beta'^2}{Z_{\text{s}}^{1/2}\beta} \tag{18}$$

This is the interaction energy corresponding to the weak adsorption limit.

The interaction energy decreases with increasing delocalization of the surface electrons. The larger the width of the surface local density of states, the lower the interaction energy. This result also implies that the energy of interaction with a coordinatively unsaturated surface (small z_{s}) is larger than to a higher coordinatively saturated surface. When the parameter

$$\mu = \frac{\beta'^2}{z_{\text{s}}\beta^2}$$

which measures the relative value of adatom surface atom interaction versus that between the metal atoms, increases, the Lorenzian electron energy distribution on the adatom broadens and changes shape (see Fig. 2). A double peaked structure evolves, which can become wider than the valence electron energy band of the surface. The doubly peaked energy distribution indicates the formation of a surface molecule. The low-energy peak corresponds to the binding part of the electron density, the high-energy portion of the distribution corresponds to the antibonding part of the electron density. Similar features arise in the local density of states of the surface atom due to its interaction with the adatom (Fig. 3). The bonding and antibonding electron density in the surface molecule is also controlled, to a significant extent, by the contribution of the surface electron density. In the surface molecule limit,

$$\frac{\beta'^2}{z_{\text{s}}\beta^2} \gg 1$$

with α_0 be equal to E_{F} the interaction energy becomes:

$$E_{\text{int}}^{\text{s}}(E_{\text{F}} = \alpha_0) = 2\beta' \tag{19}$$

This is the same result that would be derived from the recombination of a free surface atom and the adsorbate orbital. Now, as also sketched in Fig. 2, two sharply defined energy states appear outside the surface electron energy band. The energies correspond to the bonding and anti bonding molecular orbitals of the surface complex. The first order correction to eq 19 is the localization energy of an electron on a surface atom. This relates to the sublimation energy of a surface atom into the gas phase and can be easily deduced. In the near surface molecule limit the interaction energy becomes

$$E_{\text{int}}^{\text{n.s.}}(\alpha_0 = E_{\text{F}}) = 2\beta' - E_{\text{subl}} \tag{20}$$

$$\approx 2\beta' - a\sqrt{z_{\text{s}}} \times \beta \tag{21}$$

where a is a numerical constant that depends on surface electron occupation.

The localization energy is proportional to the square root of the number of surface atom neighbors and the metal–metal overlap energy integral. Again, we find that the chemisorption energy decreases with increasing delocalization of the surface electrons. In the surface molecule limit, chemisorption becomes corrosive. The metal–metal bonds next to the surface complex weaken.

The results discussed so far are generally valid even when more sophisticated computational approaches are used. Critical to the results discussed so far is the assumption that only bonding orbital fragments between adsorbate and surface are occupied. We will now show that the results can qualitatively change when antibonding orbital fragments become occupied. This becomes especially relevant when one is interested in differences in adsorption energy as a function of surface atom coordination number. This is the subject of the next topic which analyzes chemisorption to the (111) surface of a face centred cubic metal. The adsorbing molecule can choose between four different adsorption sites: atop, twofold, and two threefold sites.

For higher coordination sites, eqs 9 and 10 are no longer valid for evaluating $\Gamma(E)$. One now has to find the linear combination of surface atomic orbitals, that correspond to the local symmetry of the adsorption site. These are the group orbitals $\varphi_{\text{g}}^{\text{s}}$ [8, 9]. The surface atom local density of state in eqs 9 and 10 are now replaced by group orbital local density of states $\rho_{\text{s}}^{\text{g}}(E)$. For instance, in twofold coordination, two s atomic orbitals from each surface atom are combined to form the surface group orbital

$$\phi_{\text{g}}^{\text{s}} = \frac{1}{\sqrt{2}}(\varphi_1^{\text{s}} + \varphi_2^{\text{s}})$$

References see page 957

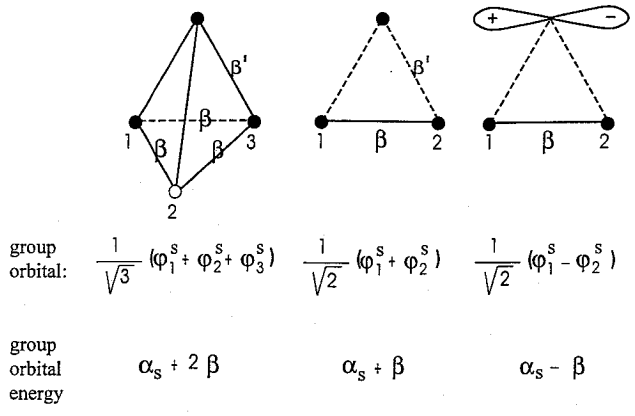

Figure 4. Group orbitals and their energies.

and the group orbital density of states

$$\langle \phi_g^s | \delta(E - H_s) | \phi_g^s \rangle$$

The overlap energy integral becomes

$$\langle \varphi_0 | H | \phi_g^s \rangle = \sqrt{2}\beta'$$

The general expression for $\Gamma(E)$ is now

$$\Gamma(E) = n\pi\beta'^2 \rho_s^g(E) \tag{22}$$

where n is the coordination number of the adsorbate. For this more general case, the interaction parameter μ becomes

$$\mu = \frac{n\beta'^2}{z_s\beta^2} \tag{23}$$

It might be expected that the linear dependence of μ on n would lead to a linear dependence of the interaction energy between adsorbate and surface coordination number n. This is, however, only the case in the limit of weak adsorption ($\mu \ll 1$) and when bonding adsorbate–surface orbital fragments are occupied.

It is found in the surface molecule limit that the bonding orbital is the low-energy solution of the equation

$$(\alpha_0 - E) - \frac{n\beta'^2}{\alpha_s + x(n)\beta - E} = 0 \qquad \begin{cases} n = 1; & x(n) = 0 \\ n = 2; & x(n) = 1 \\ n = 3; & x(n) = 2 \end{cases} \tag{24}$$

Equation (24) corresponds to the clusters depicted in Fig. 4. The group orbital and its group orbital energy are also listed for the situation where an asymmetric p orbital interacts with surface s atomic orbitals in a twofold coordination site.

In the surface molecule limit the bonding orbital fragment energy becomes

$$E_g^b = \alpha_s + \sqrt{n}\beta'. \quad (\alpha_m = \alpha_s = \alpha) \tag{25}$$

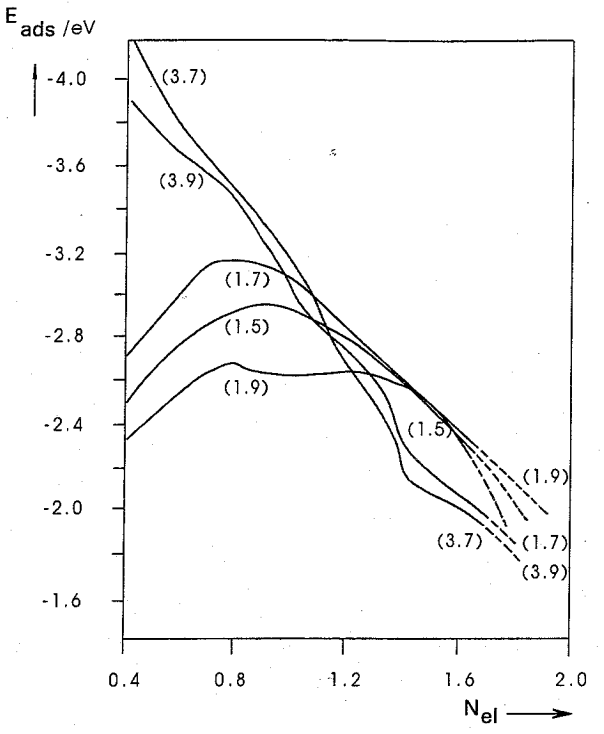

Figure 5. Bethe lattice results. Interaction energies of onefold, twofold, and threefold adsorbed hydrogen, as a function of Bethe lattice atomic orbital electron occupation. For the points (a, b); a is the hydrogen atom coordination number; and b the number of Bethe lattice neighbor atoms nearest neighbor of atom involved in the adsorption bond.

The binding energy is proportional to the square root of the adatom coordination number. The apparent preference for higher coordination sites strongly depends on the distribution of electrons over bonding and antibonding absorbate–surface atom fragment orbitals. When the electron occupation of antibonding orbitals dominates, low coordination sites may become preferred.

This is illustrated by a set of model calculations which use the Bethe lattice approximation to describe the embedding of a surface cluster in a metal lattice. Each metal atom is represented by one s atomic orbital and the interaction energy with a hydrogen atom is computed for varying metal electron occupation. This simulates the analogous change in d bond filling of transition metals. This implies that the metal Fermi level now varies as a function of surface orbital electron occupation. The electron–electron interaction between the electrons on the adsorbate therefore had to be explicitly included in the calculation. The calculation results are shown in Fig. 5.

According to the Newns–Anderson model [2] in the weak adsorption limit ($\mu \ll 1$), the paramagnetic state on hydrogen becomes most stable. In Fig. 5 the regime where this occurs (high metal valence band electron

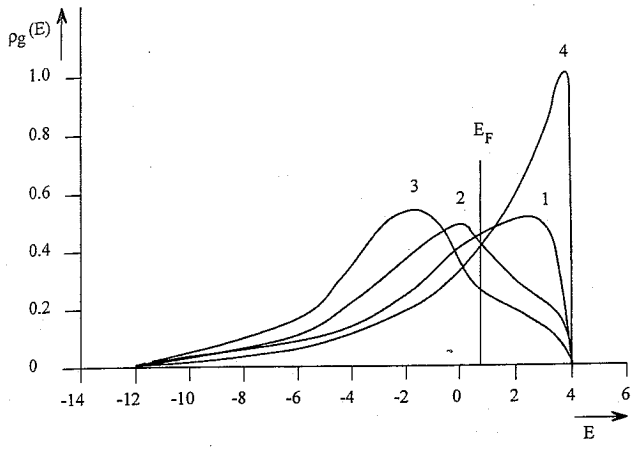

Figure 6. Group orbital local density of states on Bethe lattice representing (111) surface of face centred cubic lattice [18]:

1. Surface group orbital local density of states of single atomic orbital.
2. Surface group orbital local density of states of group orbital

$$\frac{1}{\sqrt{2}}(\varphi_1^s + \varphi_2^s)$$

3. Surface group orbital local density of states of group orbital

$$\frac{1}{\sqrt{2}}(\varphi_1^s + \varphi_2^s + \varphi_3^s)$$

4. Surface group orbital local density of states of group orbital

$$\frac{1}{\sqrt{2}}(\varphi_1^s - \varphi_2^s)$$

occupation) is indicated with broken lines. Results presented are for hydrogen adsorbed atop, twofold, and in threefold coordination. The metal surface atom coordination number is also varied, in order to compare adsorption between open and more dense surfaces.

Within the surface electron density regime presented, it is found that the interaction energy for the atop described configuration moves through a maximum value (actually a double maximum) and that the interaction energies for the twofold and threefold coordination sites decrease with metal valence electron occupation. At low valence-electron occupation where only bonding adsorbate–metal fragment orbitals are occupied, the expected preference for bonding is for high coordination sites.

This leads to higher interaction energies for the open surface. However, as the valence electron occupation increases, both these trends invert. This inversion arises from the now very different distribution of electrons over bonding and antibonding surface fragment orbitals for the same metal valence electron occupation. This is due to the very different group orbital local density of states of the surface electrons that interact with the adatom when surface coordination is varied. The corresponding group orbital LDOS at different coordination sites are shown in Fig. 6.

Embedding of the surface complex clusters into the Bethe lattice leads to a broadening of the group orbitals electron densities. This is due to electron delocalization. The maximum surface group electron density moves to lower energy with increasing adsorbate coordination number, similar to the corresponding group orbital energy in the isolated metal clusters (Fig. 4). As a consequence, when comparing bonding at the same surface, i.e. constant value of E_F, the antibonding adsorbate–metal surface fragment orbitals for the atop geometry are less occupied than those that correspond to the high coordination geometries. Therefore when the electron occupation increases, the bond energies for the high-coordination sites will decrease more readily than those for the low-coordination sites.

The emphasis of the tight-binding approximation is on covalent binding aspects. Effects due to electrostatic screening are more appropriately handled by in the jellium model descriptions, to be discussed next.

C The Free-Electron Approach to Chemisorption: Jellium Model

Within the free-electron approximation the discrete attraction potentials due to positive nuclei are replaced by a continuous electrostatic background. The charge density is chosen such that attraction by the electrons is equal but opposite in sign to the electron–electron repulsion energy. This is the so-called jellium model. It is possible to combine a free-electron calculation for the s and p valence electrons with a tight-binding description for the interaction with the d valence electron bond. This is the essence of effective medium theory [9]. The advantage of free-electron theory is that explicit expressions for kinetic, exchange, and correlation energy are known as a function of electron density. In contrast to the tight-binding approaches, electrostatic interactions can be described rigorously within free-electron models. Density functional theory (DFT) approaches, which include accurate descriptions of the discrete atomic potentials have been implemented in sophisticated computational schemes and predict adsorption properties in close agreement with experiment. They are regarded as computational extension of the free-electron/tight-binding methods [10]. The exchange and correlation energy functionals used are based on jellium-type expressions. Using the variational principle, differential equations for the wave functions can be formulated, and solved for limited and infinite systems.

The first success of the jellium model was the prediction of the work function changes as a function of adsorbate concentration. The presence of a surface can be simulated within this model by choosing a coordinate, such that the positive background potential $V_b(r)$ is positive when $x < 0$, but equal to zero when

References see page 957

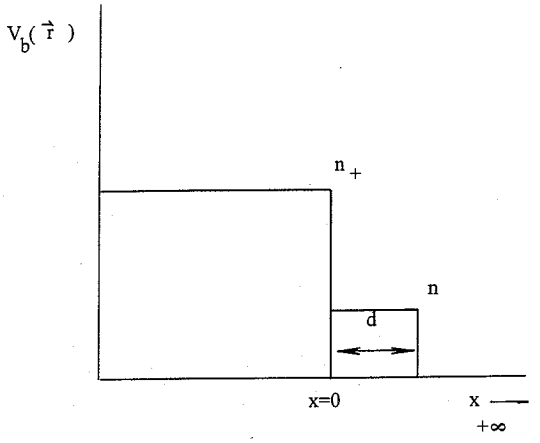

Figure 7. Potential energy at a surface with low electron density atom adsorbed according to the free-electron model (schematic).

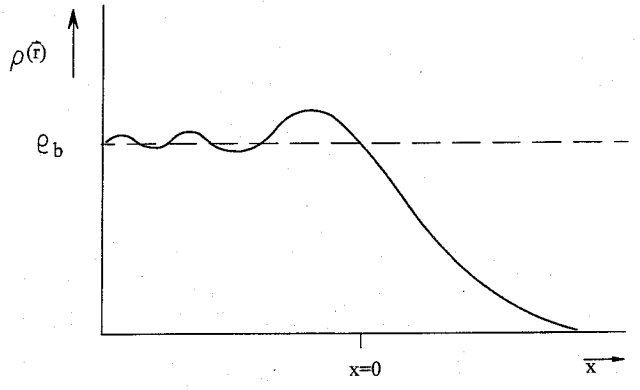

Figure 8. Electron density profile near a surface, x is the surface plane.

$x > 0$. If the electron density remained unchanged up to the surface defined by $x = 0$, $V_b(r)$ would be equal to $-n_+$. This is sketched in Fig. 7.

However there is a spillover of electrons due to their finite kinetic energy and the real electron density generates a surface dipole. This is depicted schematically in Fig. 8.

Adsorption of an atom, as for instance an alkali atom, can be simulated by adding additional potential density (see Fig. 7), corresponding to that of the adatom. A lower potential will result in electron backflow from the adsorbate into the metal, resulting in a reduced work function. A higher potential will attract electron density with an opposite effect. The charge that develops on the adsorbate is screened by electron-electron attractions. For instance a negative overall charge in the regime $0 < x < d$, will push away surface electrons so that a positive charge δ develops. The resulting image potential attraction is

$$E_{\text{im}} = -\frac{\delta^2}{4r + \lambda} \tag{26}$$

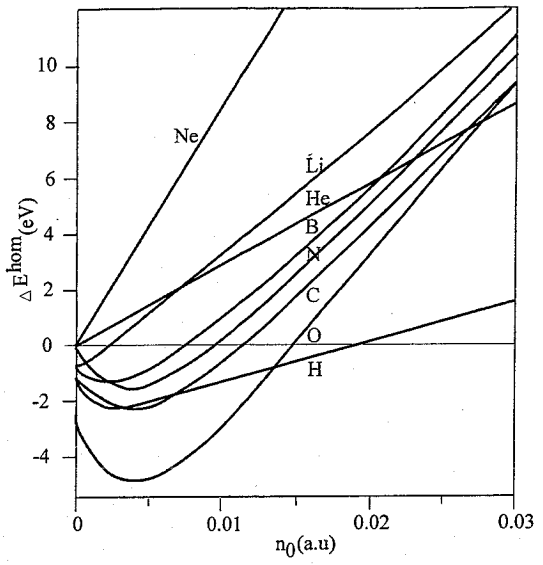

Figure 9. Embedding energies of He, H, Li, B, N, C, O, and Ne in a homogeneous electron gas as a function of electron gas density [11].

where r is the adsorbate surface distance and λ the free-electron screening length. A similar result is found for a positive charge, which will attract electrons. This image charge screening effect will therefore alter the effective energy levels of adsorbate molecules bound to conductive surface. Charges become stabilized due to the induced image potentials. The basic idea of effective medium theory [9] is to replace the density of an adsorbing atom by that of the jellium substrate. The embedding energy,

$$\Delta E = \Delta E^{\text{emb}}[n_0(\vec{r})]$$

is equal to the difference in energy between the combined atom and host system minus that of the separated atom and the host, where $n_0(\vec{r})$ is the density of the host. Curves for $\Delta(E)^{\text{emb}}$ are shown in Fig. 9. As expected the interaction with Ne is repulsive, due to Pauli repulsion even at very low densities. For oxygen, the attractive interaction reaches a maximum for a particular density because it will readily accept electrons. Above the substrate density that corresponds to the interaction energy maximum antibonding adsorbate metal surface orbitals become occupied.

In effective medium theory, the interaction energy includes an induced image potential interaction term computed from the free-electron part. The contributions from d-electron interactions computed within the tight-binding model discussed in subsection B are explicitly included. The effective medium theory, while still approximate, is quite powerful because of the inclusion of electrostatic terms. It has especially been very useful in the analysis of alkali coadsorption effects [12].

D The Quantum Chemistry of Chemisorption

Hoffmann has been instrumental in developing and demonstrating the extension of the tight-binding approximation to relate the surface electronic structure to the nature of the chemisorbed state [5]. This is implemented in his extended Hückel (EHT) molecular orbital approach, which has been extensively used to analyze and understand chemisorption in many different catalytic systems. The simplicity of the EHT approach makes it quite easy to explore how changes in electronic structural parameters affect changes in chemisorption. This is certainly an advantage for this approach. The main limitation of the approach is that it can only provide qualitative results and trends. Quantitative results require more extensive, first-principle theoretical treatments. Nonetheless many important insights and concepts about chemisorption can be explored in the framework of the EHT approach. Many of these concepts can then be further verified by more detailed quantitative *ab initio* or density functional methods as will be discussed. We review here the chemisorption of CO and CH_3 to illustrate the quantum chemical description of chemisorption. The EHT method uses the same functional form of the one-electron wave functions described for the tight-binding approach in eqs 1 and 3. The extended Hückel method explicitly includes nonorthogonality of the atomic orbitals (eq 4). The important interaction term that depends on orbital overlap, S_{ij}, is Pauli repulsion. This is responsible for the repulsive part of the potential energy curve for the interaction energy of a chemical bond. Pauli repulsion arises for the exclusion principle that states that electrons of the same spin cannot occupy the same orbital.

As illustrated in Fig. 10, inclusion of orbital overlap leads to larger destabilization of antibonding orbitals than bonding orbitals. Hence when bonding as well as antibonding orbitals are occupied, the overall interaction becomes repulsive. In the interaction between s atomic orbitals. Pauli repulsion is linear in the coordination number of the adsorption site:

$$E_{\text{rep}}(\text{Pauli}) \approx 4n(\beta' - \alpha S)S \approx 4nS^2 \qquad (27)$$

Hence Pauli repulsion favors bonding to low coordination sites.

The attractive part of the chemisorption energy can be found from the interaction between occupied fragment orbitals and unoccupied fragment orbitals (frontier molecular orbital theory). This is illustrated in Fig. 11.

In the weak interaction limit, the attractive part of the potential energy curve can be computed from second-order perturbation theory. For the simple atomic metal orbital system, the corresponding expression is

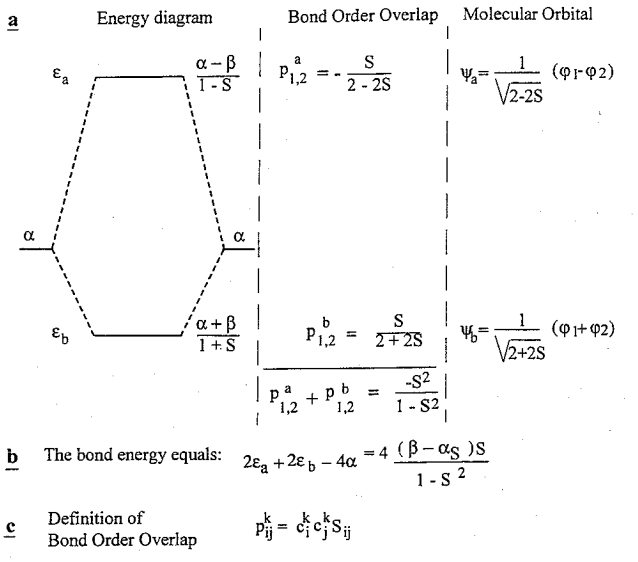

Figure 10. Extended Hückel molecular orbitals and energies for hydrogen.

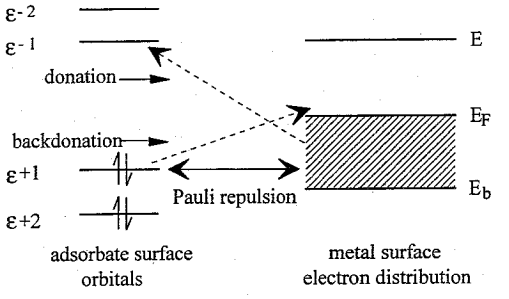

Figure 11. Frontier molecular orbital scheme for adsorbate–surface interaction.

given in eq 28. It is a relation that depends on the group orbital density of states around the Fermi level multiplied by terms that depend on the electron occupation of the valence electron bond:

$$\Delta E^{w^*}_{\text{attr}}(\text{FMO}) \approx -2\bar{\rho}_g(E_F)\left(\sum_i \beta'^2_{+i} \ln\frac{E_t - E_{+i} + E_{\text{im}}}{E_F - E_{+i} + E_{\text{im}}} + \sum_i \beta'^2_{-i} \ln\frac{E_{-i} - E_F + E_{\text{im}}}{E_{-i} - E_b + E_{\text{im}}}\right) \qquad (28)$$

where w^* = weak interaction limit. Expression 28 provides an approximate relationship between the electron density near the Fermi level and the chemisorption energy. $\overline{\rho_g}(E_F)$ is the group orbital local density of states at the Fermi level averaged over an energy width of

$$\approx 2\frac{n\beta'^2}{\sqrt{z_s}|\beta|}$$

References see page 957

around the Fermi level. Relationship (28) agrees with the computed electron occupation dependence of the chemisorption energies for the different adsorption modes in Fig. 5. It parallels approximately the group orbital local density of states dependence shown in Fig. 6. Additional parameters that control the energy difference between adsorbate and metal surface orbitals, are the surface work function, adsorbate image potential, electron affinity, as well as the unoccupied and occupied surface electron density of states. Note that we explicitly introduced the image potential term, which arises from the screening of charge on the adsorbate that is generated by electron donation and backdonation. The first term of eq 28 is the contribution to the bond energy due electron donation of electrons from bonding adsorbate orbitals into empty surface orbitals. The second term arises from electron backdonation of surface metal electrons into the unoccupied adsorbate orbitals.

We will analyze the quantum chemistry of the surface-chemical bond further by the use of extended Hückel calculations of the electron energy distribution of CO chemisorbed to a large Rh cluster [13], simulating a Rh (111) metal surface. In the next section we will discuss in detail the consequences of the cluster size choices on the variation in the chemisorption bond strength. Clusters of 50 metal atoms or more reproduce the electronic structural features found for calculations on extended surface. The electronic properties of interest are the local density of states of the adsorbate orbitals or metal atomic orbitals, given by

$$\rho_i(E) = \langle\varphi_i|\delta(E-H)|\varphi_i\rangle \tag{29}$$

$$= \sum_k |\langle\varphi_i|\psi_k\rangle|^2 \delta(E-E_k) \tag{30}$$

and the bond-order overlap population (eq 31). The bond-order overlap energy density of states $\pi_{ij}(E)$ represent the atomic orbital interference terms as a function of energy and provides information on the bonding and antibonding character of the adsorbate–surface fragment orbitals.

$$\pi_{ij} = \langle\varphi_i^{\text{ads}}|\delta(E-H)|\varphi_j^{\text{surface}}\rangle\langle\varphi_i^{\text{ads}}|\varphi_j^{\text{ads}}\rangle \tag{31}$$

$$= \sum_k \langle\varphi_i^{\text{ads}}|\phi_k\rangle\delta(E-E_k)\langle\phi_k|\varphi_j^{\text{ads}}\rangle\langle\varphi_i^{\text{ads}}|\varphi_j^{\text{ads}}\rangle \tag{32}$$

In figure 12 the computed local density of states of the highest occupied molecular orbital (HOMO), 5σ and lowest unoccupied molecular orbital (LUMO) $2\pi^*$ molecular orbitals of CO adsorbed atop, twofold, or threefold coordinated to the (111) surface of Rh are presented. Due to the interaction with surface orbitals the local density of states (LDOS) distributions broaden with respect to their sharp gas-phase values. As expected, the increase in coordination extends the width of the LDOS of the $2\pi^*$ orbital. The change in the 5σ orbital is much less coordination dependant because of the directed nature of this orbital. At the atop site it will overlap significantly with surface d_{z^2} and p orbitals, as can be seen from the corresponding bond order overlap population densities (Fig. 12). In twofold and threefold coordination, however, the 5σ is directed to the surface normal instead of the surface orbital and hence has a small overlap with the surface atomic orbitals.

$\pi_{ij}(E)$ orbital occupation provides a bonding contribution to the surface chemical bond. When $\pi_{ij}(E)$ is negative, orbital occupation tends to antibonding and repulsive contributions. For the corresponding discrete bond order overlaps P_{ij}^k, this is illustrated for H_2 in Fig 10. The functions π_{ij} presented in Fig. 12 enable analysis into the extent to which s, p, and d electrons contribute to the bond energy. Note that the 5σ–d_{z^2} interaction has both bonding as well as antibonding character. A further increase in the valence electron occupation (higher E_F) will increase the occupation of antibonding orbitals and hence weaken the interaction energy. This is a very general result for the interaction of adsorbate orbitals that are doubly occupied and have a nearly filled d valence electron bond. Similar to the results depicted in Fig. 5, the interaction is a maximum when only bonding orbital fragments occupied.

The interaction decreases when the d valence electron occupation is such that bonding orbital fragments become depleted. Analysis of the $\pi_{5\sigma,d_{z^2}}$-orbital (Fig. 12 (E)) shows that the downwards-shifted 5σ orbital becomes part of the bonding surface orbitals. However, the broadened and upwards shifted $\rho_{d_{z^2}}$ surface atomic local density of states becomes part of the antibonding surface orbitals.

Opposite behavior is found for the $2\pi^*$ electron density. The $2\pi^*$ local density of states has bonding surface electron density in the energy regime of the surface d electron density. The antibonding nature of the surface electron density near the gas phase $2\pi^*$ electron energy level is also reflected in the upwards shift of this density. The $2\pi^*$–surface interaction is mainly of bonding character. For most metals only bonding surface orbital fragments are occupied. Whereas the $2\pi^*$ orbitals for the gas-phase CO molecule are not occupied, the interaction of CO with the surface broadens the CO $2\pi^*$ local density of states and leads to a partial occupation of these orbitals. The CO $2\pi^*$ orbitals are antibonding and hence their occupation will weaken the C–O interaction energy, which is experimentally reflected in a lowering of the C–O stretching frequency. The $2\pi^*$ LDOS broadens more when CO is in higher coordination sites. This leads to a larger contribution of low-energy bonding orbitals and a resulting increased $2\pi^*$ electron occupation.

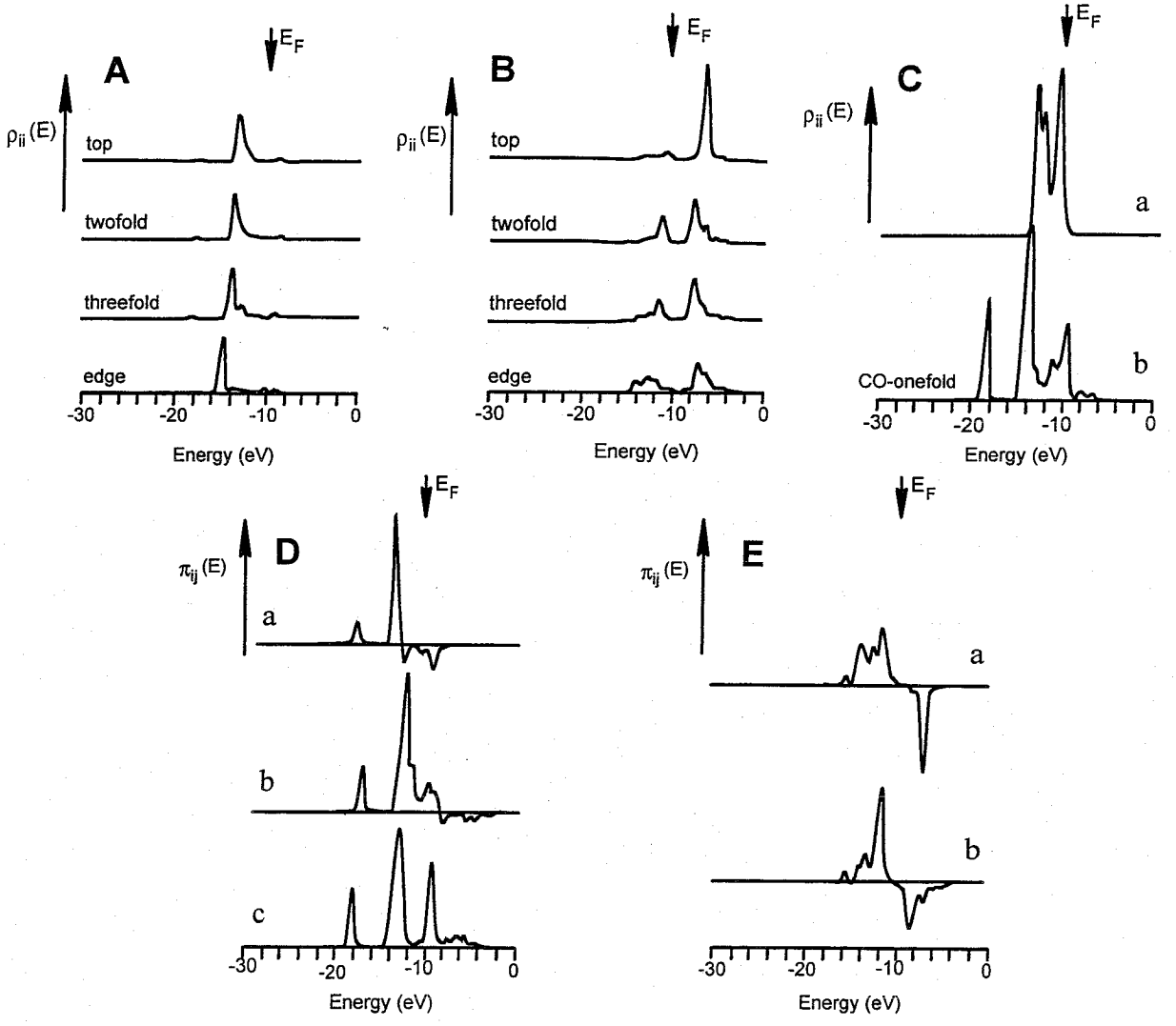

Figure 12. The electronic interactions of CO with the Rh(111) surface [13].
A. The CO, 5σ local density of states $\rho_{5\sigma}(E)$ on different adsorption sites.
B. The CO, $2\pi^*$ local density of states $\rho_{2\pi^*}(E)$ on different adsorption sites.
C. The local density of states of the surface atomic orbital d_{z^2} for CO chemisorbed atop before and after chemisorption (b).
D. Bond order overlap density of states of the CO 5σ orbital for CO chemisorbed atop: (a) $\pi_{5\sigma,d_{z^2}}$; (b) $\pi_{5\sigma,s}$; (c) $\pi_{5\sigma,p_z}$.
E. Bonder order overlap density of states of the CO $2\pi^*$ orbital for CO chemisorbed atop: (a) $\pi_{2\pi,d_{xz}}$; (b) $\pi_{2\pi,p_x}$.

The 5σ orbital has a strong bonding interaction with the surface s and p valence electrons which is dependent on the relative values of Fermi level and 5σ position. The antibonding orbital fragments can also become occupied when interacting with the surface s electrons. For CO adsorbed atop, the $2\pi^*$ CO orbitals have only a weak interaction with the surface s atomic orbitals, because of zero overlap between $2\pi^*$ and its next-neighbor s atomic orbital. For this reason p-type orbitals drive the surface adsorbates to twofold and threefold coordination sites where group orbitals of the required symmetry can favorably interact.

The resulting bonding scheme is summarized in Fig. 13. The consequence of the high occupation of antibonding 5σ–surface orbital fragments is that CO will prefer the low coordination atop site to relieve Pauli repulsion. However, the $2\pi^*$–p orbital interaction will favor the higher coordination sites.

A consequence of these opposing forces is that the differences in bond energies of Co adsorption at different coordination sites is small.

In practice, bonding with atoms such as C, O, or S, is dominated by the interaction with the adatom *p* atomic orbitals and strongly favors high coordination. Such atoms bind an order of magnitude stronger to the

References see page 957

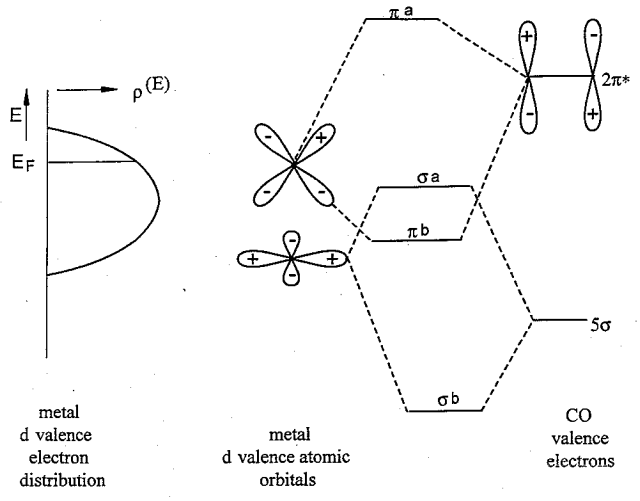

Figure 13. Orbital scheme (schematic) of the interaction of the CO 5σ and $2\pi^*$ orbitals with surface d_{x^2} and d_{z^2} orbitals.

metal surface because of the relatively low energy of the unoccupied atomic orbitals.

A general bonding trend for the transition metals in a given row of the periodic system is that there is an increase in the interaction energy in moving from right to the left (e.g. from Cu, Fe, or Ag to Ru). Three factors contribute:

(i) the d valence electron occupation decreases;
(ii) the ionization potential (work function) of the metal decreases (only true for Group VIII and early transition metals);
(iii) the spatial extent of the d valence electron increases.

The lower adsorption energies for Group IB elements compared to Group VIII elements, is due to the complete filling of the d valence electron band for the IB metals. This leads to large repulsive interactions with occupied adsorbate orbitals (e.g. the CO 5σ orbital) and occupation of antibonding orbital fragments.

5.1.2.3 Concepts in Chemisorption

A Introduction

So far we have discussed the electronic nature of the surface-chemical bond based on parametrized model considerations. The current status of computational chemistry and physics has reached a state where quantitatively reliable studies on small clusters and even transition metal slabs are feasible.

Herein, we simply outline the available first-principle-based methods for analyzing chemisorption systems. A more detailed review is available elsewhere [14]. The first is based on the ab initio Hartree–Fock approach and its successive improvements by the application of configuration interaction techniques [15]. Outstanding representatives of this approach in catalysis are Siegbahn [16], Bagus [17], Goddard [18] and their co-workers. The other first principle approach is based upon the application of density functional theory. With the incorporation of nonlocal gradient corrections to the exchange-correlation functional and the application of energy minimization techniques, this technique has the potential to become widely adapted in chemisorption theory, due to the reliability of the results and its significant savings in CPU. In addition, the development and application of DFT-slab programs allow one to treat very realistic catalytic systems. Baerends [10a], Salahub [10b], and Ziegler [10c] have made significant contributions to the development of these approaches.

Within the *ab initio* computational scheme framework, Whitten [19] has developed an interesting and useful approach, whereby small clusters (e.g. the surface complex) are embedded into a larger cluster model of the bulk, which is described by lower quality wave functions. An alternative embedding scheme has been developed by Pisani [21]. Next to the embedding schemes density functional theory applications have appeared to use extended sates to simulate the transition surfaces. For example, te Velde and Baerends were recently able to deduce highly accurate adsorption values for the adsorption of CO to Cu [21] and resolve the long-standing theoretical question of the coordination of CO to Cu, with their DFT-slab approach. Feibelman [22] used a related approach to analyze the vibrational motion of hydrogen.

Finally we have to mention the important empirical approach developed by Shustorovich [23], the bond order conservation–Morse potential (Boc–MP) method. This is a parameterized scheme that enables the estimate of adsorption energies of complex molecules based on parameters derived for those of the free molecules or adsorbed atoms.

BOC–MP theory is approximately valid for many systems. Its expressions work most satisfactory for situations where bonding is nondirectional. Each atom is assigned a particular valency. When an atom becomes coordinated to neighbors this valence is distributed over the different chemical bonds. Because the valency is constant, the larger the number of the neighbors, the smaller the energy per bond. This phenomenon is often observed in chemisorption. When a molecule adsorbs, intramolecular bonds as well as metal atom bonds of the surface atoms involved in the adsorption complex weaken. Ultimately this may lead to surface reconstruction or surface corrosion.

In this section we will revisit many of the concepts presented earlier and review their validity within the context of results based on first-principle density functional theory calculations. Elsewhere [6] we provided an extensive review of first-principle-based calculations adsorption and reactivity on transition clusters and surfaces.

B Chemisorption to Clusters

It is now widely recognized that the interaction between an adsorbing molecule and metal particle may be strongly cluster dependent. Interestingly, the cluster-size dependence is most significant for adsorption on small unoptimized metal clusters. Such clusters have been studied extensively as models of surfaces. We illustrate this cluster-size effect here for the interaction of CO with Co and Rh clusters, based on density functional theory results [24]. The question we address is what is the preferred coordination site of CO. On the dense surfaces such as Rh and Co, CO prefers atop coordination. However, as illustrated in Fig. 14(a), CO prefers the higher coordination site on small clusters that model the dense surface.

The result has been shown to be due to the response of the cluster electrons to the disturbance with CO. A bond order overlap analysis of the CO nearest-neighbor atom interaction indicates that the preference for CO bonding is for onefold coordination. Coordination differences for the Co atoms in the respective clusters result in different Co–Co interactions. This ultimately controls the overall adsorption energetics. The low Co atom coordination numbers in the clusters biases CO bonding, to high coordination sites. This is attributed to the Co electron higher electron localization energy. The choice of the spherical clusters Co_{13} (Fig. 14(b)), enables the study of the three CO coordination modes on the same clusters confirm this analysis. Now, the atop coordination of CO is found to be preferred [24].

Bond order overlap population analysis confirms the explanation proposed earlier on the basis of the extended Hückel method. The repulsive interaction between the doubly occupied CO 5σ orbital and the Co 3d valence orbitals with approximately eight electrons per atom leads to occupied antibonding admolecule–surface atom orbitals. This preferred atop interaction is only partially counteracted by the backdonating interaction with the CO $2\pi^*$ orbitals that prefer the high coordination site.

The spherical cluster is but one approach to reduce cluster-size anomalies, a second method would be to use extended surface clusters, as discussed later, whereby a large enough top layer surface exists to remove edge localization at the central sites. The importance of cluster atom coordination number is again found in density functional theory calculations of CO interacting with tetrahedral Rh_4 and Rh_{10} clusters [25]. On the Rh_4 cluster, CO coordination is preferred in twofold coordination, instead of the onefold surface coordination site, again the result is due to a low coordination of the atoms. On the large Rh_{10} cluster, CO is found to preferentially adsorb atop. The two inequivalent Rh atoms of Rh_{10} cluster enable us to test the relation between admolecule bond energy and surface atom local density of states bandwidth. The LDOS distribution of

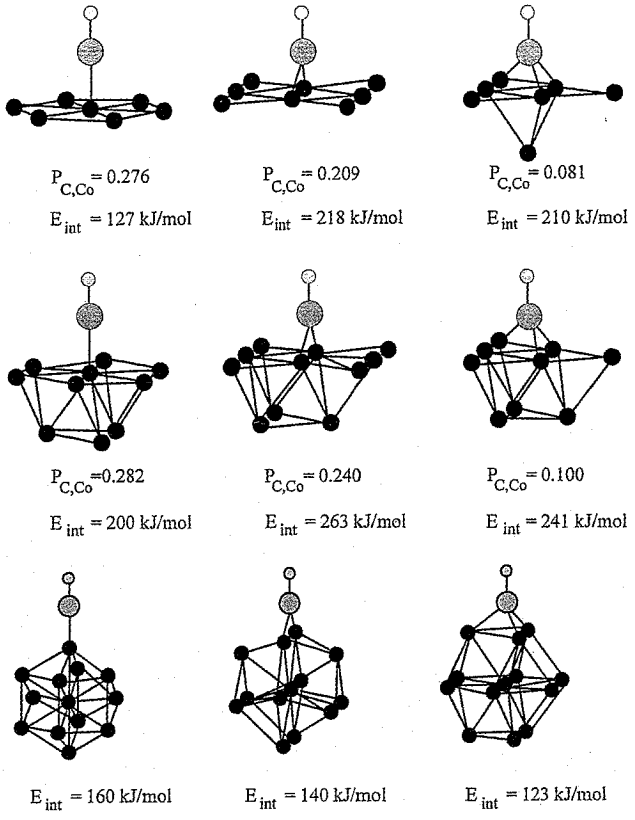

Figure 14. Interaction energies and bond orders of CO adsorbed to different Co clusters [24]. The bandorder overlap occupations are computed from

$$P_{ij} = 2\sum_{k}^{\text{occ.}} P_{ij}^{k}$$

the valence electrons of the Rh atom, with three Rh neighbors and the Rh atom in the middle of the tetrahedral edge with six Rh neighbors are also shown in Fig. 15. Also given are the interaction energies of CO on the two Rh atoms. CO is found to interact most strongly with the coordinatively most unsaturated Rh atom. Its local density of states distribution has the smallest degree of delocalization.

It follows from the analyses in the previous section, that the cluster-size dependence will be stronger for the more weakly bound adsorbates (as molecules) than the strongly interacting atoms, when the surface complex energy is large compared to the electron localization energy. The computed dependence of adsorbate interaction energy on cluster size is now well documented experimentally. For small particles fluctuations in cluster-size interacting energy are observed that appear to correlate with cluster ionization potential [26]. Interaction energies appear to converge to surface values for clusters of the order of 20 atoms or more.

References see page 957

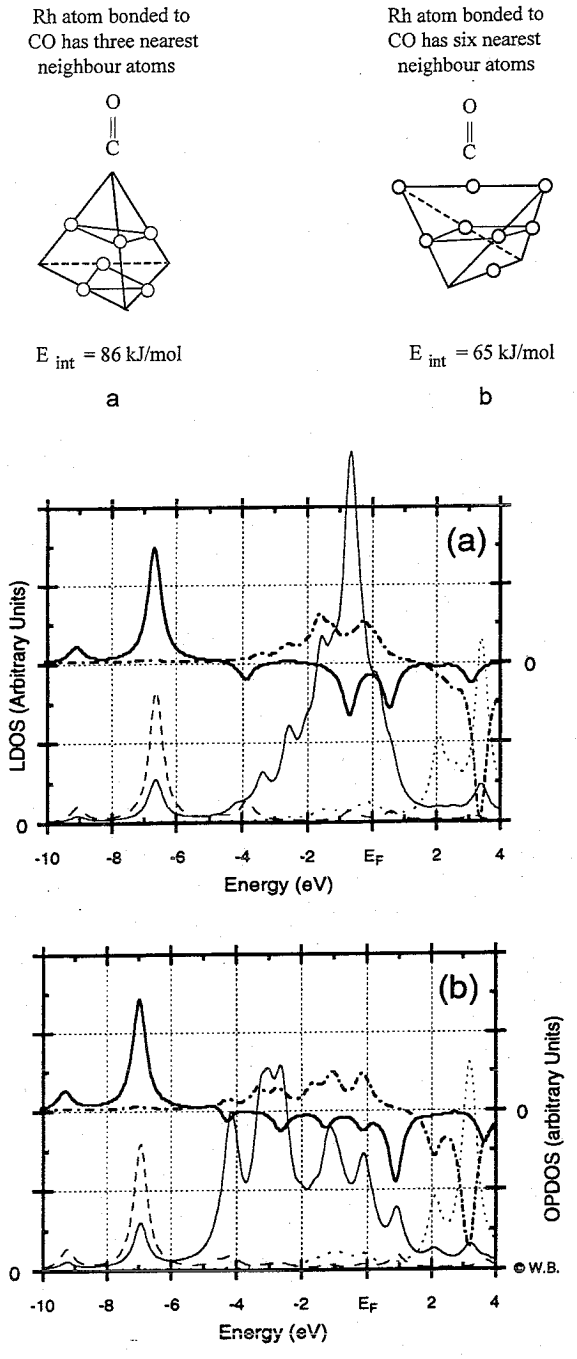

Figure 15. CO chemisorbed atop to a Rh_{10} cluster [25]. The local densities of states ρ of Rh 4d, CO 5σ and CO $2\pi^*$, and the bond order overlap population densities π_{ij} between the rhodium and CO orbitals for onefold CO adsorption on Rh_{10}. Adsorption on Rh (3*nn*) is shown on the left (a) and adsorption on Rh (6*nn*) is shown on the right (b). Each graph shows: (———) LDOS of Rh; (- - - -) LDOS of CO 5σ; (·····) LDOS of CO $2\pi^*$; (———) BOOPD between Rh–CO 5σ; (– – – –) BOOPD between Rh–CO $2\pi^*$.

Interestingly, recent results suggest that interaction energies converge at smaller cluster sizes for nonlocal density functional calculations provided that both the adsorbate as well as the cluster are optimized and that the proper spin state is chosen [10b, 27]. For example, Neurock et al. [27] found that chemisorption energies for atomic hydrogen and oxygen on the octahedral Pd cluster depicted in Fig. 16 are within 15 kJ mol^{-1} of the experimental values for hydrogen and oxygen on Pd (111). Figure 16 depicts the optimized structures for Pd_6 bare, Pd_6 with hydrogen, and Pd_6 with oxygen. The bare Pd_6 cluster was found to be most stable as a triplet. This follows known evidence that the Pd dimer is also triplet and that palladium bulk is paramagnetic. Geometry optimization of the bare Pd_6 cluster transformed the starting octahedral cluster into one which essentially has C_{4v} symmetry. There are four short planar Pd–Pd bonds of 2.63 Å and six long Pd–Pd bonds of 2.76 Å.

Adsorption of H or O forms strong bonds with the surface palladium cluster which subsequently alters the cluster bond lengths. The strong Pd–H and Pd–O bonds lead to weaker Pd–Pd cluster bonds between the Pd atoms involved in the adsorption complex.

The effect of the extended surface was examined by optimizing a bare Pd_{18} cluster model and a hydrogen Pd_{18} model [27]. Results depicted in Fig. 17 demonstrate that the Pd_{18} structures bond by pushing the central three palladium atoms in the surface upwards. Qualitatively, the results are very similar to those for Pd_6. Due to constrained nature of the surface, however, the changes are less dramatic for the Pd_{18} cluster. The elevation of the surface atoms involved in the adsorption complex is well established in surface science literature. Van Hove and Somorjai [28], for example, have clearly shown that ethylidine adsorbed on Pt leads to longer Pt–Pt bonds and a lifting of these atoms out of the surface plain by about 0.12 Å.

More generally these changes in the local geometry at (or near) the chemisorption site will lead to local stresses which could ultimately lead to surface reconstruction effects [29].

C Lateral Interactions

The interaction between atoms or molecules coadsorbed to a transition metal surface may be repulsive as well as attractive. Figure 18 illustrates three different coadsorption situations for adatoms (N and O), adintermediates (OH and NH), and molecules (NH_3 and O_2) on a (111) surface. The interaction energies were computed using density functional theory with nonlocal gradient corrections for both exchange and correlation.

They illustrate that the interaction energy between coadsorbed atoms or intermediates is repulsive, when they share a covalent bond with a surface atom. The repulsive interaction is significantly larger when they share two rather than one surface atom. The nature of the interaction energy is a strong function of the relative position of the adsorbates.

In the case of coadsorption of O and NH_3 (case I), the interaction energy of NH_3 is increased when it is

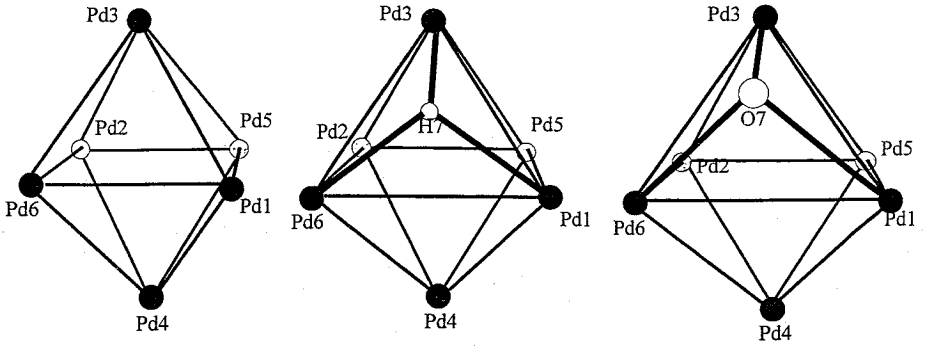

triplet doublet triplet

Pd_6–Triplet		Pd_6H–Doublet		Pd_6O–Triplet	
1–3	2.756	1–3	2.918	1–3	3.131
1–6	2.631	1–6	2.898	1–6	3.074
3–6	2.756	3–6	2.918	3–6	2.918
2–4	2.756	2–4	2.667	2–4	2.651
2–6	2.632	2–6	2.756	2–6	2.757
4–5	2.757	4–5	2.661	4–5	2.628
		Pd–X 1–7	1.768	1–7	2.068
		3–7	1.768	3–7	2.068
		6–7	1.767	6–7	2.068

Figure 16. Structures and bondlengths (Å) for geometrically optimized Pd_6 clusters. Free hydrogen atom adsorbed and O adsorbed clusters are compared [27].

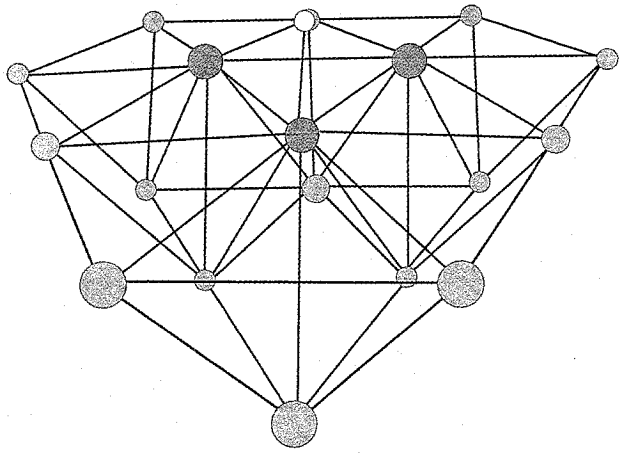

	Pd_{18} fixed	Pd_{18} Opt
Pd - H	1.78	1.75
Pd - Pd		
Local - local	2.75	2.82
Local - local	2.75	2.72

Figure 17. Pd_{18}-H cluster: Bond distances (Å) are compared for locally geometry-optimized and not geometry-optimized cluster atom positions.

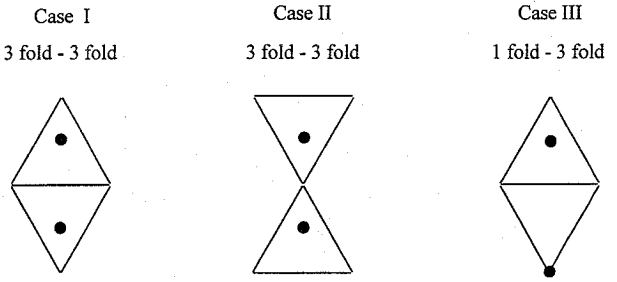

Species	Case I	Case II	Case III
NH_3 on Cu(8,3)-O	-	-	-32
NH_3 on Cu(8,3)-O	-	-	-17
NH_2 on Cu(8,3)-OH	-	-	-5
NH on Cu(8,3)-O	211	25	-
N on Cu(8,3)-O		30	-
N on Cu(8,3)-OH	170	29	-

Oxygen and hydroxyle are always threefold coordinated

Figure 18. Interaction energies between adsorbed atoms on a Cu surface [30].

References see page 957

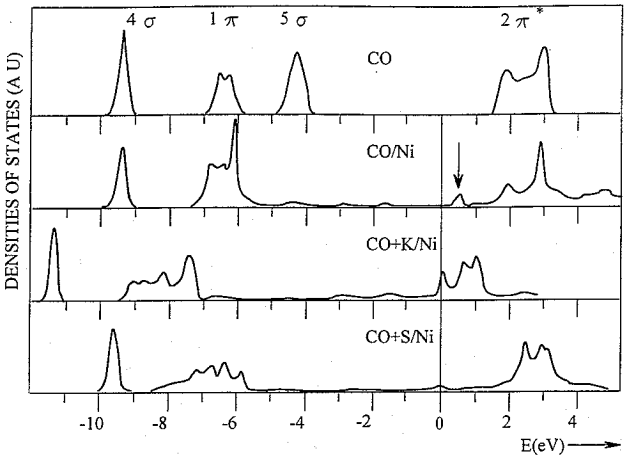

Figure 19. Linear augmented plane wave results of the local density of states of CO adsorbed on Ni(111) [32]: (a) unsupported CO film; (b) CO adsorbed on nickel; (c) CO adsorbed with potassium on nickel; (d) CO adsorbed with sulfur on nickel.

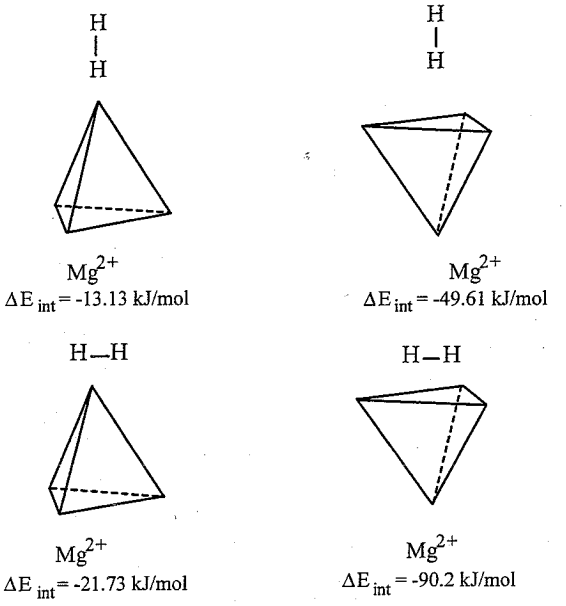

Figure 20. Changes in the interaction energies of H_2 with Ir_4 clusters due to the presence of a Mg^{2+} ion [35].

bound to a surface atom next to the surface atom Cu–O adsorption complex. The adsorption energy is increased by $30\,kJ\,mol^{-1}$ [31]. The weakening of the Cu–Cu bonds next to the cu atom involved in the surface bond with the oxygen bond results in a decreased delocalization energy of the Cu electrons associated with the Cu atom to which NH_3 is bonded. Lateral interactions can be also electrostatic in nature. In the case of ammonia interacting with the coadsorbed oxygen atom, 10% of the interaction energy originates from the direct electrostatic attraction between the negatively charged oxygen atom and positively charged ammonia. The covalent interaction energies rapidly decline with distance. Within the jellium model the interaction energy has been found to decrease as r^{-3}. Lateral interactions can also be dominated by electrostatic interactions. This is, for instance, the case when alkali atoms are coadsorbed to a metal surface. Using the augmented plane wave approximation for CO and K coadsorbed to Ni, Wimmer et al. [32] convincingly demonstrated the existence of a strong electrostatic interaction. This can be deduced from the relative shifts of the Co electronic levels when CO is adsorbed to Ni in the presence and absence of potassium (Fig. 19).

The positive charge of potassium lowers the work function of the metal surface and hence lowers the CO electronic levels compared to those of the Ni-electrons. The result is an enhancement of the backdonation of electrons into the CO $2\pi^*$-orbitals. The donating interaction for the CO 5σ-orbitals is reduced in the presence of coadsorbed potassium. The enhancement of the backdonation into the CO $2\pi^*$-orbitals changes the relative energy enough to alter the preferred CO-coordination sites. For instance on the Pt (111)-surface it has been shown that CO-shifts from the atop position to a high coordination site [33, 34].

When a small metal particle is adsorbed next to a cation, as in a zeolite or on an oxidic support, the electrostatic field of such a cation will polarize the metal particle. This is illustrated in Fig. 20 for an Ir_4 particle adsorbed next to a Mg^{2+} ion. The changes in the interaction energy of H_2 with the Ir_4 particle are shown. The interaction energy of H_2 with Ir_4 (measured by DFT calculations) is weak. There is a strong Pauli repulsion between the double occupied $H_2\sigma_g$ orbital and the occupied Ir_4 orbitals. Bonding becomes more favorable for H_2 adsorbed to a single Ir atom. In the presence of the Mg^{2+} ion, there is a polarization of Ir_4 which removes electron density from between the adsorbed H_2 molecule and interacting Ir atoms. As a consequence Pauli repulsion is reduced and now the hydrogen atoms can approach the Ir atoms so that strong orbital overlap and develops backdonation of Ir electrons into the $H_2\sigma_\mu^*$ becomes possible. The interaction energy of H_2 with Ir is now enhanced and adsorption parallel to the Ir particle in threefold coordination becomes favored.

5.1.2.4 The Surface Chemical Bond: A Summary

Chemisorption causes significant changes in local electronic structure, that in the case of strong interactions often leads to surface rearrangements. The structural changes can often be understood as a consequence of bond order conservation. The more bonds there are to an atom the weaker the other bonds associated with this atom become.

The adsorbate bond strength follows from the distribution of electrons over bonding and antibonding

fragment orbitals. The interaction with the s and p metal surface valence electrons usually favors the high coordination site. The d valence electron interaction, however, can be repulsive, which would favor low coordination. The adsorption energy tends to increase with *d* valence electron depletion.

The adsorption energy of a molecule can be considered as controlled by a balance of donating and backdonating interaction terms. For backdonation, the interaction between adsorbate unoccupied orbitals and the metal surface favor high coordination. For donation, the interaction favors low coordination. The d valence electron interaction controls the balance of these two effects. Adsorbed atoms with accessible p atomic orbitals, favor high coordination. The preference for site coordination is much less for adsorbed molecules.

Weak, as well as strong chemisorption locally disturb the electronic structure and geometry of the surface atoms close to the adsorbate molecule. The chemical bonds between surface atoms involved in the adsorption complex and neighboring surface atoms weaken, dependent on the strength of the adsorbate–surface interactions.

The substrate disturbance by an adsorbate is strongly surface or cluster-size dependent. This strongly affects the overall interaction energy and leads to surface and particle size-dependent interaction energies. Surface relaxation effects enable adsorption complexes to take on geometries very similar to those in the analogous organometallic coordination complexes.

As the adsorbate concentration increases the intra-atomic surface bonds become weaker. This can subsequently lead to surface reconstruction effects. The lateral interaction between the adsorbates give rise to nonideal mixing and order–disorder transitions of the surface layer [36]. Surface atoms with lower surface atom coordination numbers tend to be more reactive than surface atoms with a higher coordination numbers due to the larger electron delocalization associated with the latter. Atoms bind more strongly and tend to prefer adsorption in high coordination sites, whereas molecules adsorb more weakly with smaller differences in the interaction energies of different coordination sites. When donative interactions dominate and the contributions from the d valence electron band is strong, there will be a tendency towards atop coordination. The details strongly depend on the distribution of the valence electrons over surface metal d, s, and p electrons.

When bonding adsorbate–surface orbital fragments are occupied, higher coordination tends to be favored. Occupation of antibonding adsorbate–surface orbital fragments favors bonding to lower coordination sites. It is important to consider changes in Pauli repulsion (due to the antibonding orbital interactions) as well as the backdonative and donative interactions when analyzing changes in the interaction energy over different transition metal surfaces.

A decrease in work function will favor backdonative interactions, and hence increase the bond energy. However, donative interactions will decrease and the overall interaction result will depend on the balance of the two changes. For adatoms the backdonative interaction dominates, so that the bond energy increases. For molecular adsorbates such as CO, the balance is more subtle. For instance, CO binds more strongly to Pt than to Ni, because on Pt the donative interaction dominates. This agrees with the CO preference for atop coordination. On Ni, however, the backdonative interaction dominates, resulting in a preference of CO for higher coordination sites.

A decrease of the transition metal d valence electron occupation will decrease the occupation of antibonding adsorbate–surface fragment orbitals and hence assist the increase in bond energy when comparing bonding to metals across a row (from right to left) in the Periodic Table. This increase in interaction energy is also partially due to the increase in spatial extension of the d orbital band, that favors overlap with adsorbate orbital.

The low reactivity of the Group IB metals (Cu, Ag, Au) compared to that of the Group VIII Ni, Pd, and Pt metals stems from the repulsive interaction between adsorbate orbitals with the filled d valence electron band of the IB metals. The resulting decrease in the interaction energy is not compensated for by an increase in the backdonating interactions due to the lowering of the work function of the latter.

Alloying of a Group VIII transition metal with a Group IB metal leads to changes in bond energies of adsorbates, because now mixed surface ensembles of Group IB and Group VIII surface atoms are formed. New mixed-metal surface sites also exist. This may reduce the interaction energy of adsorbates in high coordination sites, because multiple coordination to the more strongly interacting Group VIII surface atoms can now become suppressed (secondary ensemble effect) [36].

References

1. J. Koutecky, *Phys. Rev.* **1957**, *108*, 13.
2. D. M. Newns, *Phys. Rev.* **1969**, *178*, 1123.
3. T. B. Grimley in *Critical Review in Solid State Science*, CRC, **1976**, 239.
4. J. R. Schrieffer in *Dynamic aspects of Surface Physics*, Proc. Int. School of Physics 'Enrico Fermi', course XVII, Bologna, **1974**.
5. R. Hoffmann, *Solids and surfaces, a chemist's view of bonding in extended surfaces*, VCH New York, **1988**.
6. R. A. van Santen, *Theoretical Heterogeneous Catalysis*, World Scientific, Singapore, **1991**.
7. J. R. Norskov, N. D. Lang, *Phys. Rev.* **1980**, *B21*, 2136. J. K. Norskov, *Phys. Rev.* **1982**, *B26*, 2875.

8. R. A. van Santen, *J. Chem., Soc. Faraday Trans. 1*, **1987**, *83*, 1915.
9. M. C. Zonnevylle, R. Hoffmann, P. J. van den Hoek, R. A. van Santen, *Surf. Sci.* **1989**, *233*, 233.
10a. E. J. Baerends, A. Rozendal, in *Quantum Chemistry: the challenge of transition metals and coordination chemsitry* (Ed.: A. Veillard), Reidel, Dordrecht, **1986**, p. 159; P. M. Boerrigter, G. te Velde, E. J. Baerends, *Int. J. Quantum Chem.* **1988**, *33*, 87.
10b. A. St. Amant, D. R. Salahub, *Chem. Phys. Lett.* **1990**, *169*, 387; D. R. Salahub, R. Fournier, P. Meynaski, I. Papai, A. St. Amant, J. Ushio in *Theory and Applications of Density Functional Approaches to Chemistry*, (Eds: J. Labadowski, J. Andrelon), Springer, Berlin, **1991**.
11. M. J. Puska, R. M. Nieminen, M. Manninen, *Phys. Rev.* **1980**, *B24*, 3037.
12. S. Holloway, J. K. Norskov, N. D. Lang, *J. Chem. Soc., Faraday Trans. 1* **1987**, *83*, 1893.
13. R. V. van Santen, A. de Koster *Stud. Surf. Sci. Catal.* **1991**, *64*, 1.
14. R. A. van Santen, M. Neurock, Catal. Rev. **1995**, *37*, 557. F. Ruette (Ed.), *Quantum chemistry approaches to chemisorption and heterogeneous catalysis*, Kluwer, dordrecht, **1992**; E. M. Shustorovich (Ed.), *Metal–surface Reaction Energetics: Theory and Applications to Heterogeneous Catalysis, Chemisorption and Surface Diffusion*, VCH, New York, **1991**; R. V. van Santen, E. J. Baerends in *Theoretical treatment of large molecules and their interactions* (Ed.: Z. B. Maksic) Springer, 1991, Part 4, pp. 323–390.
15. A. Szabo, N. S. Ostland, *Modern Quantum Chemistry*, MacMillan, New York, **1982**.
16. P. E. M. Siegbahn, U. Wahlgren in *Metal-surface Reaction Energetics: Theory and Applications in Heterogeneous Catalysis, Chemisorption and surface diffusion*, VCH, New York, **1991**.
17. P. S. Bagus, K. Hermann, *Phys. Rev.* **1986**, *B33*, 2987; P. S. Bagus, F. Illas, *Phys. Rev.* **1990**, *B42*, 10852.
18. T. H. Upton, W. A. Goddard, *CRC Critical Review in Solid State and Materials Sciences* **1981**, *261*; E. A. Carter, W. A. Goddard, *J. Catal.* **1980**, *112*, 80; E. A. Carter, W. A. Goddard, *J. Phys. Chem.* **1988**, *92*, 2109.
19. J. Whitten in *Cluster Models for Surface and Bulk phenomena*, (Eds: G. Pacchioni, P. S. Bagus, F. Parnigiani,) NATO ASI series, 375 **1991**, A. Chattopadhyay, H. Tang, J. L. Whitten, *J. Phys. Chem.* **1990**, *94* 6397; H. Yang, J. L. Whitten, *J. Chem. Phys* **1989**, *91*, 126.
20. T. B. Grimley, C. Pisani, *J. Phys. C.* **1974**, *7*, 2831; C. Pisani, *Phys. Rev.* **1978**, *B17*, 3143; R. A. van Santen, L. H. Toneman, *Int. J. Quantum Chem.* **1977**, Suppl *2*, 83.
21. G. te Velde, E. J. Baerends, *J. Comp. Phys.* **1992**, *99*, 84.
22. P. J. Feibelman, *Surf. Sci.* **1994**, *299/300*, 426.
23. E. H. Shustorovich, *Surf. Sci. Rep.* **1986**, *6*, 1.
24. M. C. Zonneviylle, J. J. C. Geerlings, R. A. van Santen, *J. Catal.* **1994**, *148*, 417.
25. W. Biemolt, Ph.D Thesis, Eindhoven, **1995**.
26. A. Kaldor, C. M. Cox, M. Zakin, *Adv. Chem. Phys* **1988**, *70*, 211.
27. M. Neurock, G. Coulston, D. Dixon, unpublished results.
28. U. Starke, A. Barbieri, N. Materer, M. A. van Hove, G. A. Somorjai, *Surf. Sci.* **1993**, *286*.
29. J. K. Norskov, *Rep. Progr. Phys.* **1998**, *53*, 1253; J. K. Norskov in *The Chemical Physics of Solid Surfaces and Heterogeneous Catalysis*, (Eds. D. A. King, A. P. Woodruff, Elsevier, **1993**, vol 6.
30. M. Neurock, R. A. van Santen, W. Biemolt, A. P. J. Jansen, *J. Am. Chem. Soc.* **1994**, *116*, 6860.
31. W. Biemolt, A. P. J. Jansen, M. Neurock, G. J. C. S. van de Kerkhof, R. A. van Santen, *Surf. Sci.* **1993**, *287/288*, 183.
32. E. Wimmer, C. L. Fu, A. J. Freeman, *Phys. Rev. Lett.* **1985**, *55*, 2618.
33. G. E. Crowell, E. L. Garfunkel, G. A. Somorjai, *Surf. Sci.* **1983**, *121*, 203.
34. R. A. van Santen, Proceedings of the 8th International Congress on Catalysis, Springer, Berlin, **1984**.
35. E. Sanchez Marcos, A. P. J. Jansen, R. A. van Santen, *Chem. Phys. Lett.* **1990**, *167*, 399; A. P. J. Jansen, R. A. van Santent, *J. Phys. Chem.* **1990**, *94*, 6764.
36. V. P. Zhdanov, *Elementary Physics Chemical Processes on Surfaces*, Plenum, New York, **1991**.
37. W. M. H. Sachtler, R. A. van Santen, *Adv. Catal.* **1977**, *26*, 69.

5.2 Microkinetics

5.2.1 Rates of Catalytic Reactions

M. Boudart

5.2.1.1 Introduction

Catalysis is a kinetic phenomenon. The study of kinetics in catalysis started early in the 20th century in a phenomenological mode. The first study of this kind dealt with the rate of decomposition of stibine SbH_3 on the surface of antimony, a product of the reaction acting as a catalyst. The kinetic data of Stock and Bodenstein [1] were fitted to what became known as an empirical power rate law:

$$v = k[SbH_3]^n \qquad (1)$$

where the rate v is proportional to the concentration of the gas phase reactant to a fractional power n with empirical values 0.55, 0.56, 0.63, and 0.65 at 273, 298, 323, and 348 K, respectively. The kinetics of this historical reaction have been discussed repeatedly [2].

The carly phenomenological period of catalytic kinetics was followed by a second mechanistic period based on the findings of Langmuir. A highlight of this period was the publication in 1931 of a very influential book by Schwab that was translated into English by Taylor and Spence [3]. During the 1920s and 1930s, the kinetics used in heterogeneous catalysis were based largely on the Langmuir lattice model of a surface consisting of identical noninteracting adsorption sites. These so-called Langmuir kinetics were developed first by Hinshelwood [4] and then by Hougen and Watson to become a systematized tool for process research and development in the 1940s and 1950s [5]. The idea was to assume a reaction mechanism leading to the best data fitting rate equation for use in catalytic reactor design and operation. In time, the data fitting proce-